Eur. Phys. J. B **43**, 463–470 (2005)
DOI: 10.1140/epjb/e2005-00079-5

THE EUROPEAN PHYSICAL JOURNAL B

Resonant valence-band photoemission spectroscopy on the $Fe_{62}Ni_{20}Cr_{18}$ alloy

V. Formoso[1,a], G. Chiarello[1], R.G. Agostino[1], L. Papagno[1], E. Colavita[1], L. Floreano[4], R. Gotter[4], A. Morgante[3], A. Santaniello[2], and A. Verdini[4]

[1] Istituto Nazionale di Fisica della Materia (INFM) and Dipartimento di Fisica, Università della Calabria, 87036 Rende-Cosenza
[2] Sincrotrone Trieste, Basovizza, 34012 Trieste, Italy
[3] Dipartimento di Fisica, Università di Trieste, Via Valerio 2, 34127 Trieste, Italy
[4] TASC, INFM, Area di Ricerca, Basovizza, 34012 Trieste, Italy

Received 13 October 2003 / Received in final form 5 October 2004
Published online 30 March 2005 – © EDP Sciences, Società Italiana di Fisica, Springer-Verlag 2005

Abstract. The $Fe_{62}Ni_{20}Cr_{18}$ valence band was studied by scanning the photon energy across the $2p_{3/2}$ core-level threshold of each element of the alloy. A resonant enhancement of the weak 3*d*-like features was observed. In pure transition metals, similar valence band resonances are explained by a radiation-less Raman de-excitation emission, which is active at threshold and degenerate with the two-hole satellite of direct photoemission. Present structures are associated to satellite features occurring in $Fe_{62}Ni_{20}Cr_{18}$, and their intensities and binding energies are compared to those of the pure metal components. The alloy satellite resonant behaviour reveals some peculiar modifications of: a) the crossover between the radiation-less Raman scattering and the Auger emission regimes; b) the ratio of the relative intensities of the main and satellite peaks. We mainly assign these differences to the hetero-nuclear bonds in the alloy.

PACS. 79.60.-i Photoemission and photoelectron spectra – 81.05.BX Metals, semimetals, and alloys

1 Introduction

Alloys are an important class of materials with a peculiar surface chemical reactivity, which makes them good candidates for technological applications in the field of heterogeneous catalysis [1–3]. Many industrial catalysts consist of solid surfaces with several metallic elements since alloy materials have more specific and effective chemical properties than pure metals. Several studies [4–7] have shown that the formation of hetero-nuclear metal-metal bonds in bulk or surface compounds have a profound effect on the intra-atomic density of the electronic states of each metal alloy component. A common effect observed in bulk, as well as at surfaces, is an energy shift of the core levels due to a net charge transfer between component atoms of the alloy. However, theoretical studies [4,7] showed that the charge transfer picture does not fully account for the measured core level shifts and line shapes, which are often due to many body final state processes. On the other hand, for bulk alloys made of transition metals, there is a strict correlation between core level shifts and the density of *d* electrons located at each metal component [4,5].

In the present work we studied the electronic structure of the $Fe_{62}Ni_{20}Cr_{18}$ alloy by valence band (VB) resonant photoemission measurements at the $2p_{3/2}$ core level thresholds of Ni, Fe and Cr. Resonant photoemission spectroscopy [8–10] is exploited in condensed matter to get information on the electronic state localisation, coupling between initial and final states, and, in the case of compounds, on any electronic modification induced by hetero-nuclear chemical bonds. Experimentally [11], the resonant processes give rise to intensity enhancements of specific regions of the valence band, when the impinging photon energy is swept through the energy of a core level. A rigorous description [12] of the phenomenon would consider the excitation-decay process at the core-level threshold as a whole process connecting initial and final states. A simpler picture considers, instead, subsequent independent steps. In the latter picture, the enhancement is caused by the overlapping or, possibly, the interference between direct VB photoemission and other decay paths following the core-level excitation and leading to the same final state of photoemission. In other words, the direct photoemission channels from the valence band may add to, or interfere with the concomitant auto-ionisation channel. Of course, any detection of the considered decay path depends crucially on its probability as compared to the core-hole life-time. In the case of weakly interacting systems like Ar/Pt (111), it was shown that the coupling of Ar and empty substrate states above E_F represents a mechanism for delocalisation [13]. If the transition probabilities of the

[a] e-mail: formoso@fis.unical.it

direct photoemission and de-excitation channels are comparable, their interference leads to the characteristic Fano resonance [14]. Strong Fano modulations are observed in valence band photoemission at the $3d$ core level threshold of several transition metals and Fano-like modulations are observed at $3p$ and $2p$ core level thresholds of several transition metals and their oxides [9–11,16].

Applying more recent theoretical [3,15] and experimental [16–18] approaches to resonant photoemission, a more advanced understanding of the process is now available. Weinelt et al. [16] performed resonant measurements at the $2p$ core level threshold of Ni demonstrating that the interpretation of the experimental data needs to distinguish between two different processes, which behave differently with photon energies: the so called Radiation-less Raman (RR) scattering regime, that occurs, via virtual excited states, at the $2p_{3/2}$ core level threshold (starting already for photon energies at the onset of absorption), and the Auger (A) regime, that in the absence of multi-electron effects is expected to take place as soon as a screened core-ionised state is created ($2p_{3/2}$ photoemission binding energy). In general, neither the onset nor the maximum of absorption coincide with the $2p$ X-ray photoemission (XP) binding energy, because many body effects (correlation, screening) affect both the absorption and photoemission processes in different ways. For Cr and Fe metals, the crossover from the RR to the Auger regime is observed before the XAS maximum, at and below BE, respectively. For Ni [17], the crossover occurs at the absorption edge maximum because of peculiarities of the XAS process in Ni, e.g., the absence of correlated holes at the Ni Fermi level.

In the RR regime, the kinetic energy of emitted electrons increases linearly versus the photon energy and thus each resonant structure is observed at constant binding energy. Moreover, in the Auger regime the kinetic energy (of the Auger electrons) depends on the excitation energy, and each feature is revealed at variable binding energy. Within the above multiple step picture, the Auger regime is favoured as long as the delocalisation time of the whole process is shorter than the core-hole life time [15,19].

Recent photoemission measurements [19] at the Cu $2p_{3/2}$ edge, moreover, show that the Radiation-less Raman effect is also present for excitations to the continuum of states. Thus, RR scattering can be related to excitations to delocalised/itinerant states, and the resonant photoemission and RR scattering are general features of photoemission, independently of the degree of the electron localisation in the system [19].

In the present paper we report on a resonant photoemission study of a single crystal of $Fe_{62}Ni_{20}Cr_{18}$. The element specificity of the technique was used to separate the contributions of each alloy component within the VB photoemission yield by means of the local character of core-level threshold excitations. We found that the intensity of some features of the $Fe_{62}Ni_{20}Cr_{18}$ valence band were strongly dependent on the impinging photon energy. In particular, by scanning the photon around the Ni and Fe $2p_{3/2}$ edges, we clearly observed the development of a strong resonance feature in agreement with the well-known satellites of the respective pure metals. The binding energy of these emission peaks initially remains at a constant value up to some photon energy below the absorption edge maximum, according to the existence of a RR channel in the alloy, and, thereafter, disperses linearly with the photon energy. A much weaker Cr satellite is observed by scanning the photon around the Cr L3 edge, nevertheless it follows the same dispersion of the iron and nickel RR and A features.

The binding energies of the satellites and their intensity dependence on the photon energy were also investigated to look for possible modifications of the correlation energies upon the alloy formation.

2 Experimental

The experiments were performed at the INFM beam line ALOISA [20] of the ELETTRA synchrotron radiation source in Trieste, Italy. The spectra were recorded at normal emission by a hemispherical electron analyser described elsewhere [21] and the X-ray beam was impinging on the sample surface at a grazing angle less than 10 degrees. All the measurements were taken with transverse magnetic light polarisation i.e. electric field normal to the sample surface. This geometry enhances the relative weight of the photoemission over the Auger signal. By using a pass energy of 30 eV, the electron contribution to the total energy resolution was about 0.5 eV. The photon energy was changed in steps of about 0.15 eV over an interval of about 10 eV centred in the energy region of the $2p_{3/2}$ absorption edges of Ni, Cr and Fe. The ALOISA monochromator was operated with an energy resolution of about 0.2 eV since it is crucial to use a photon beam energy resolution narrower than the absorption line width [15] for resonant Auger measurements. In the present experiment these conditions were always fulfilled.

The $Fe_{62}Ni_{20}Cr_{18}$ single crystal was grown by Metal Crystal and Oxides (Cambridge-UK). The ternary alloy has a cubic structure and the face exposed to the synchrotron light was (111), as revealed by X-ray diffraction analysis. Order and cleanliness of the crystal surface were checked by RHEED and XPS techniques. The surface was prepared by several cycles of mild sputtering and annealing procedures. Oxygen, carbon and sulphur contaminants, initially present, were reduced to a trace levels. The base pressure during measurements was less than 3.9×10^{-8} Pa.

The annealing procedure did not affect the nominal bulk concentration of the alloy components at surface within a few %, as deduced by a specific XPS check.

3 Results

Valence band photoemission spectra of the alloy, taken for photon energies around the $2p_{3/2}$ core-level threshold of Ni, Fe and Cr, are shown in Figure 1. In each case, resonant intensity modulations are observed. Comparing the

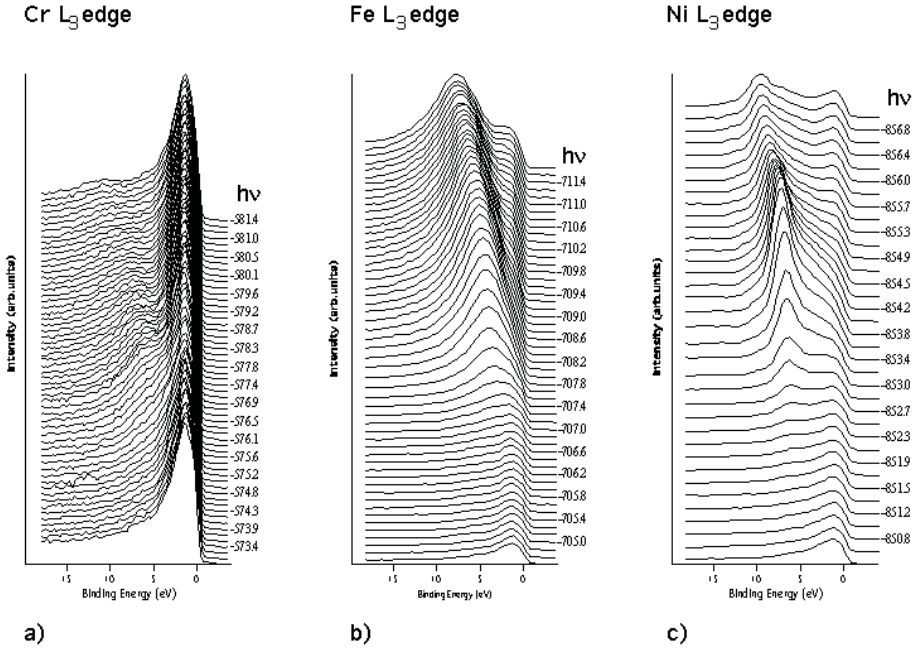

Fig. 1. Two dimensional representation of the valence band photoemission spectra of the $Fe_{62}Ni_{20}Cr_{18}$ sample across the L_3 edge of Cr (a), Fe(b) and Ni (c), respectively.

three series of spectra among them and with the analogous spectra of pure metals [16,17], quite marked differences can be singled out in the resonant behaviour.

Starting from the spectra taken at the Ni-$2p_{3/2}$ core-level threshold, (Fig. 1c), we observe already at the lowest photon energies a feature close to the Fermi level (EF) mainly due to $3d$ electrons, and a satellite feature at 6.3 eV. The intensity and the binding energy of the former peak do not depend on the photon energy. The latter structure is first observed at fixed binding energy and then shifts versus photon energy while its intensity increases significantly. Specifically, it remains at a nearly constant binding energy up to $h\nu = 853.2$ eV and, then, moves towards higher binding energies with a linear dependence on photon energy. The satellite intensity enhancement at the RR/A crossover is about 2.64 times the off-resonance valence band intensity maximum (VBIM) and continues to increase up to $h\nu = 854.0$ eV (maximum of the absorption) and then attenuates visibly. As already mentioned, this behaviour is explained by the presence of two different processes at threshold: the radiationless Raman and the Auger regimes.

The spectra of Figure 1b were acquired by varying the photon energy across the Fe-$2p_{3/2}$ core-level threshold. At low photon energies, the valence band shows electron emission essentially at the Fermi level, but, moving the photon energy towards the absorption edge maximum, the RR- feature appears at about 4.2 eV below EF. By increasing the photon energy, it remains at constant binding energy up to $h\nu = 707.8$ eV (crossover between RR and Auger regimes) and, successively, moves linearly to higher binding energies. The peak intensity increases up to $h\nu = 709.3$ eV (Fe absorption maximum) and then slowly decreases; it is about 3.23 times the off-resonance VBIM at $h\nu = 707.8$ eV.

The valence band spectra for the Cr-$2p_{3/2}$ core-level threshold, Figure 1a, mainly consist of a feature close to EF, and a weaker shoulder at higher binding energies; both intensities are scarcely dependent on photon energy.

In order to make the RR-satellite behaviour more evident, we subtracted a spectrum taken at a photon energy well below the expected resonance region from each set of spectra (see Figs. 2a, 3a, and 4a). This procedure shows the presence of the satellite at about 4.6 eV also in Cr. It is weaker than the Ni and Fe satellites, but it shows a similar behaviour versus the photon energy. The satellite energy remains fixed up to $h\nu = 575.0$ eV (Cr crossover in the alloy), while the peak intensity grows to $h\nu = 576.2$ eV (Cr absorption maximum in the alloy). The satellite intensity is 15% larger than the off-resonance VBIM at the RR/A crossover.

4 Discussion

The origin and the photon energy trend of Ni, Fe and Cr RR-satellites in pure elemental samples are well known [16,17] and are assigned to a two-hole valence band final state [9] which is reached through the RR channel. It turns out that the Auger channel becomes energy degenerate with the RR channel at a core level threshold. In the binding energy representation the different photon energy dependence of the two events is responsible for a splitting into two distinct maxima, with the Auger feature moving away from the constant-binding-energy RR feature for increasing photon energies. The Auger channel opens for photon energies before the absorption edge maximum for

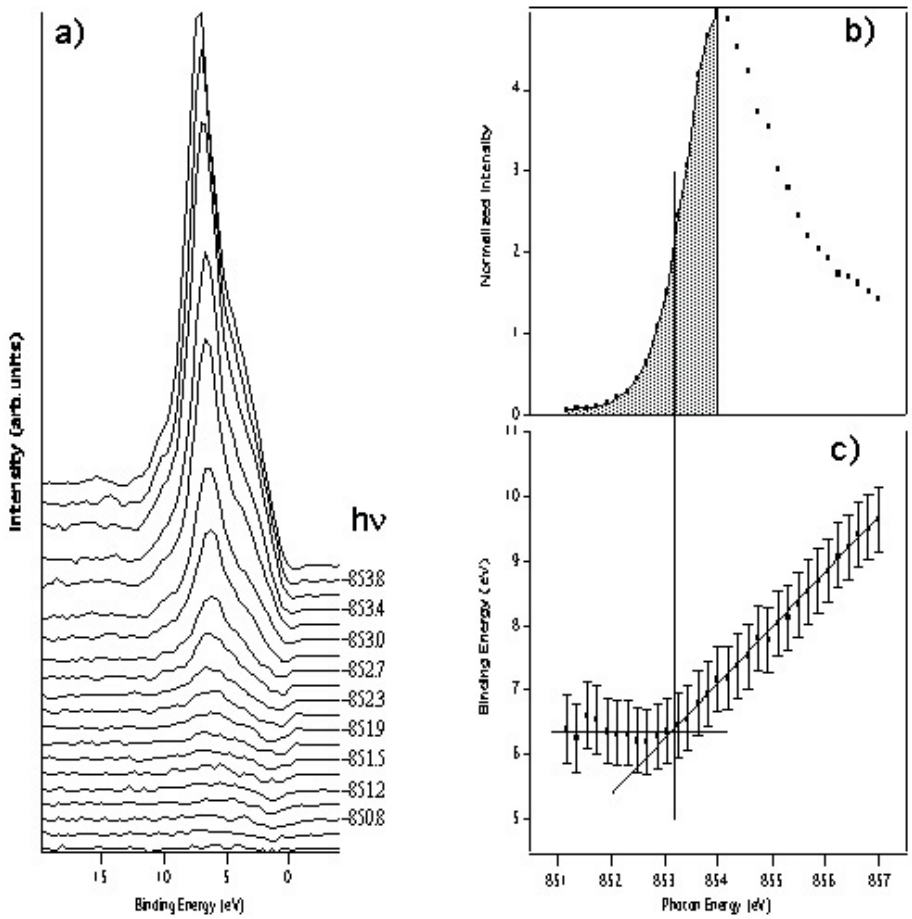

Fig. 2. a) Selected valence band spectra measured at photon energies ranging from off-resonance to the maximum of the Ni L_3 absorption coefficient. The spectra shown are the result of the removal of the off resonance spectrum from the acquired spectra of Figure 1c. b) The Ni L_3 absorption profile: the shadowed region corresponds to the photon energies of the spectra shown in a). c) Binding energy dispersion versus the photon energy of the Ni satellite position: straight lines are placed as a guide for the eye in correspondence of the average binding energy in the RR regime and at fixed kinetic energy in the Auger regime.

each elemental constituent of the alloy, and for Cr and Fe metals [17]. Interestingly, it is observed at the absorption edge maximum for Ni metal [17]. A comparison with the $2p$ XP binding energies, available for Ni, Fe and Cr metals, shows that the Auger channel opens at the $2p$ XP binding energies for Cr and Ni, which corresponds to the creation of a screened core-ionised final state that can relax by the Auger effect. In general, this energy does not coincide with the absorption maximum, since some additional hole-hole correlation energy is needed in order to create the absorption state. This is actually observed for Cr and Fe, for which some hole-hole correlation energy is responsible for the difference between the XP binding energy and the absorption maximum. In the case of Ni, instead, the BE and absorption edge maximum coincide [17], indicating that the final state of $2p$ photoemission and absorption are the same, and the XAS process can be viewed as a one-particle process.

The features observed in $Fe_{62}Ni_{20}Cr_{18}$ at the $2p_{3/2}$ core edge of each alloy component behave similarly. Although their general trends are consistent with literature findings in the pure metals, some peculiar differences allow us to single out specific aspects of the metal bond formation in ternary alloy compounds as compared to their parental metals, stressing that VB resonant photoemission measurements can show those electronic modifications induced by the alloy bonding at each elemental site.

Figure 2 shows (a) the Ni valence band spectra after the subtraction of the off-resonance spectrum, (b) the Ni $2p_{3/2}$ absorption spectrum and (c) the binding energy dispersion of the Ni RR satellite and Auger peak versus photon energies. As shown in Figure 2c, the line at a constant binding energy of 6.3 eV $\pm$ 0.5 eV represents the energy of the RR enhanced satellite peak, while the energy of the Auger yield is the line at constant slope. The onset of the energy dispersion occurs at the intersection of the two linear slopes and represents, within the estimated uncertainty error, the crossover energy between the two regimes. We notice that, unlike pure Ni [17], the crossover does not coincide with the absorption maximum, but occurs at about 0.8 eV below it. This suggests that the X-ray absorption cannot be considered as a one-particle process for Ni in the alloy and that a

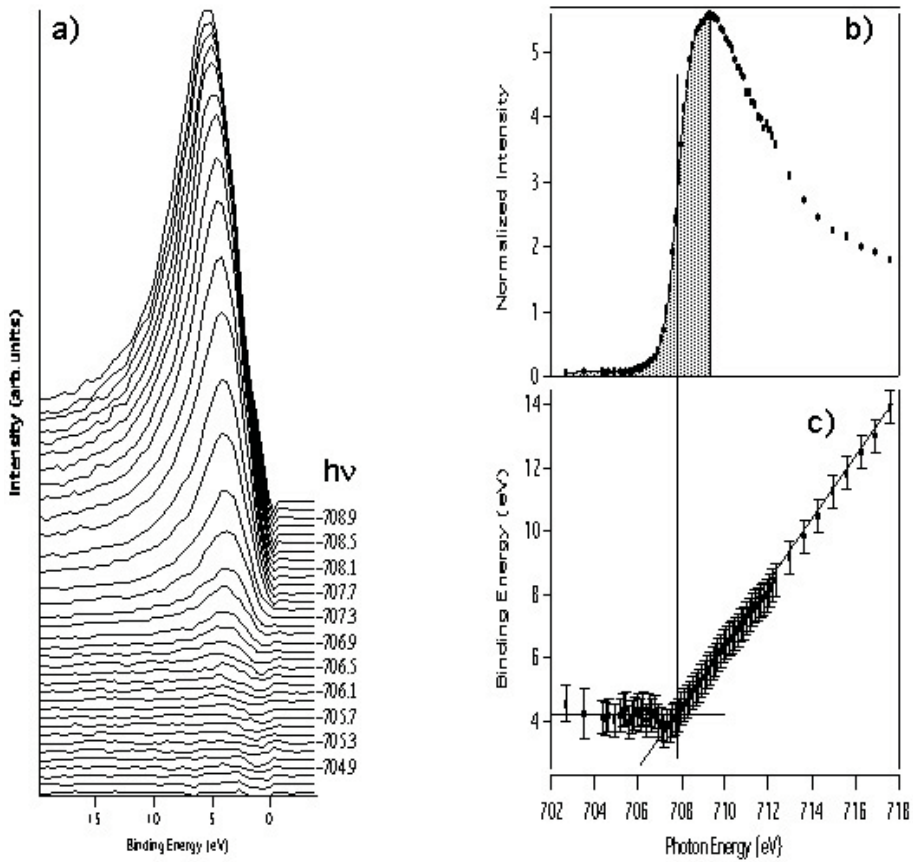

Fig. 3. a) Selected valence band spectra measured at photon energies ranging from off-resonance to the maximum of the Fe L_3 absorption coefficient. The spectra shown are the result of the removal of the off resonance spectrum from the acquired spectra of Figure 1b. b) The Fe L_3 absorption profile: the shadowed region corresponds to the photon energies of the spectra shown in a). c) Binding energy dispersion versus the photon energy of the Fe satellite position: straight lines are placed as a guide for the eye in correspondence of the average binding energy in the RR regime and at fixed kinetic energy in the Auger regime.

considerable fraction of Ni atoms of the alloy have more than one d-hole in the ground state. In addition, the rapid evolution into an Auger feature indicates some delocalization of the two holes-state in the valence band, as follows also from the similar interpretation [16,17] done for pure transition metals with partially filled d-bands. We also note that the measured energy of the Ni satellite (6.3 eV in the alloy against 6.0 eV in pure Ni) shows an almost equal binding energy of such multi-electron excitation within the uncertainty error.

The above findings suggest some delocalisation of the alloy states at Ni sites, though some charge transfer from Ni to the neighbouring atoms cannot be excluded. Of course, detailed calculations on complex systems, such as our alloy, would be necessary for a more quantitative description of the data. However, within the present phenomenological framework, we can suggest that by alloying, Ni valence states mix to the neighbouring Cr and Fe states, leading to both a small charge transfer and a $3d$ level spreading. The whole result should give rise to a decrease of the correlation energy and an invariant value for the satellite binding energy. This framework is also consistent with the findings on Fe and Cr, as discussed in the following.

The iron satellite at 4.2 eV $\pm$ 0.5 eV, Figure 3, shows behaviour very similar to that of Ni in $Fe_{62}Ni_{20}Cr_{18}$. It overcomes the main peak at EF, starting the transition from the RR- to the A-regime well below the absorption maximum (about 1.5 eV, as in Fe metal), and occurs at higher binding energy, almost 1.0 eV, than the satellite of the pure metal. It is worth noting that the absorption maximum is considered here and in the following just as a convenient reference energy. Unlike Ni in the alloy, the Fe crossover between the RR- and A-regime is at the same energy as in the pure metal, suggesting a similar hole correlation energy both in pure Fe and in the alloy [17]. Moreover, the strong satellite intensity further suggests that, similarly to the pure metal, the excitation states are scarcely delocalised at the Fe site. Thus, alloying does not increase delocalisation of Fe $3d$ levels, but rather induces a pure charge transfer to Fe atoms, while the hole correlation energy remains unvaried.

For Cr (Fig. 4), the transition from the RR- to the A-regime occurs below the absorption maximum taken as a reference energy, both in the alloy and in the metal (1.2 and 2.0 eV, respectively), confirming the importance of many body effects in both materials; moreover, the binding energy of the satellite in the alloy is higher than that

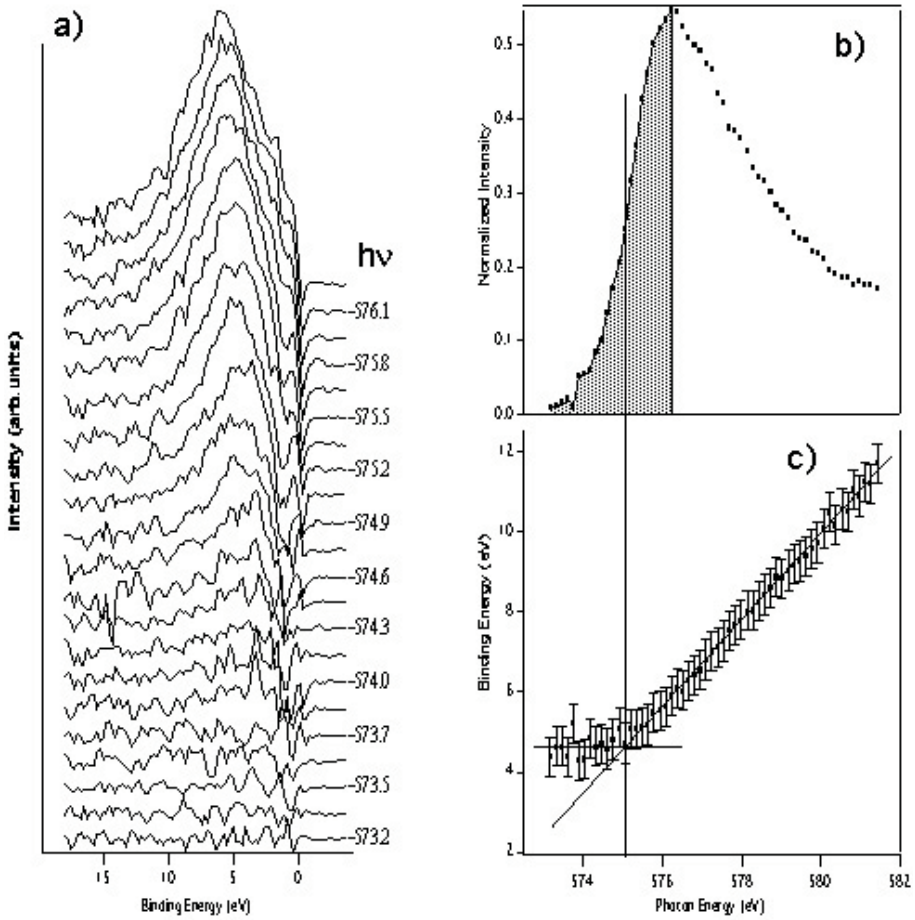

Fig. 4. a) Selected valence band spectra measured at photon energies ranging from off-resonance to the maximum of the Cr L_3 absorption edge. The spectra shown are the result of the removal of the off resonance spectrum from the acquired spectra of Figure 1a. b) The Cr L_3 absorption profile: the shadowed region corresponds to the photon energies of the spectra shown in a). c) Binding energy dispersion versus the photon energy of the Cr satellite position: straight lines are placed as a guide for the eye in correspondence of the average binding energy in the RR regime and at fixed kinetic energy in the Auger regime.

in pure Cr by 1.1 eV, similarly to Fe in $Fe_{62}Ni_{20}Cr_{18}$. The intensity of the satellite is quite weak in both the alloy and Cr metal at low photon energies, and increases by factors of 0.15 and 1.56 at resonance for the alloy and the metal [17], respectively. The weak resonant increase in the alloy may be due to an increased valence hole delocalisation and a decrease of the Cr correlation energy in the alloy with respect to the pure metal. A high density of Cr empty states is confirmed by absorption data in $Fe_{62}Ni_{20}Cr_{18}$, and, thus, Cr states, although of high density, should be quite delocalised with respect to the other metal sites.

Unfortunately, we do not know the $2p$ BEs of the alloy components and, thus, we cannot carry out an analysis of the transition from the RR to the Auger regime relative to the absorption maximum for each component as done for Cr, Fe and Ni pure metals [17]. Nevertheless, we can reasonably suppose that the BEs of Cr and Fe in the alloy are lower than the absorption maximum of their parent metals since Cr and Fe are expected to remain correlated hole systems even in the presence of a strong charge transfer. In the case of Ni, instead, a charge transfer upon alloying can add a hole at Ni making Ni a multiple hole system for which the BE and the absorption maximum are not expected to coincide. It is interesting to observe that according to the present model, Ni in the alloy resembles the behaviour of Cr and Fe pure metals, rather than Ni metal: the crossover and the maximum of absorption do not coincide, and the BE is likely to be lower than the absorption maximum.

A summary of the results for the $Fe_{62}Ni_{20}Cr_{18}$ alloy is reported in Table 1.

It is worthwhile observing that alloying modifies the satellite intensities of each component of the alloy. Particularly, the resonant process is highly intense at the $2p_{3/2}$ threshold of Fe, while it is almost quenched at Cr-$2p_{3/2}$ and reduced at Ni-$2p_{3/2}$ thresholds. The resonant satellite enhancements at RR/Auger crossovers, normalised to the valence band maxima of off-resonance spectra, are reported in Table 2 together with the analogous results for pure metals [16,17]. We observe that the resonant intensity enhancements as measured at RR/A crossover scale from Fe to Ni to Cr, differing from

Table 1. Summary of the present results on $Fe_{62}Ni_{20}Cr_{18}$. The estimated uncertainty error is reported for each measurement.

Metal edges in $Fe_{62}Ni_{20}Cr_{18}$	Satellite intensity	Satellite energy	Crossover between RR and Auger regimes
Cr-$2p_{3/2}$ edge	weak	4.6 ± 0.5 eV (3.6 eV for the metal)	1.2 ± 0.2 eV below the absorption maximum
Fe-$2p_{3/2}$ edge	strong	4.2 ± 0.5 eV (3.2 eV for the metal)	1.5 ± 0.2eV below the absorption maximum
Ni-$2p_{3/2}$ edge	strong	6.3 ± 0.5 eV (6.0 eV for the metal)	0.8 ± 0.2 eV below the absorption maximum

Table 2. Intensity enhancement results at RR/A crossover for each alloy element in $Fe_{62}Ni_{20}Cr_{18}$. The estimated contribution of each element to the total 3*d* DOS is scaled by the contribution of each element to *d* valence electrons. The analogous enhancement for each pure element is reported for comparison.

Element in $Fe_{62}Ni_{20}Cr_{18}$	Cr	Fe	Ni
Estimated contribution of each element to the total 3*d* DOS	13%	61%	26%
Intensity enhancement (present data)	0.15	3.23	2.64
Intensity enhancement of each pure element [16,17]	1.56	2.85	7.07

the pure metal case where they scale, instead, from Ni to Fe to Cr.

In order to establish the possible influence of the alloying formation on this behaviour, we took into account the alloy stoichiometry, the 3*d*-subshell photoionization cross-section [22] of each element and, moreover, the local character of the resonance process discussed above. We note that the ratios of the 3*d* photoionization cross-section of the alloy constituents are quite constant for the energies in the range of the experiment. Thus, the relative contribution of each element to the valence band emission is expected to remain unaltered across any of the three core level threshold excitations. Actually, the measured valence band line shapes in the off-resonance conditions are practically identical. This allows us to directly consider the maximum valence band emission in the off-resonance condition as a reference to measure the intensity resonant enhancements of each elemental constituent. On the other hand, instrumental effects on the spectrum line shape due to the energy resolution, both of the electron analyser and the photon monochromator, can be excluded as negligible for our working conditions.

If the number of 3*d* electrons for each element would be similar to that of each pure metal, that is, we assume negligible charge transfer upon alloying, we expect that Cr contributes to be about 13%, Fe to be about 61% and Ni to be about 26% of the total 3*d* DOS. These percentages are obtained upon weighting the stoichiometric numbers of the alloy by the nominal valence of the metal constituent (5, 7, 9, for Cr, Fe, Ni, respectively). Then, considering the absolute values of the 3*d* sub-shell photoionisation cross-sections, the contributions of Cr and Ni 3*d* emission to the total valence band reduce and enhance with respect to that of Fe, respectively. In other words, both stoichiometric and cross-section considerations support the experimental observation of the resonant enhancements scaling from Fe and Ni to Cr.

Table 2 summarises our findings for the intensity enhancement at the RR-A crossover of each alloy element.

Currently, radiationless Raman emission is interpreted as being related to the presence of localised intermediate electronic states [15,18], although this interpretation is in conflict with very recent experiments [19] which show RR scattering processes even for a continuum of states. In our opinion, those quasistationary intermediate states have an important role also in the resonant processes occurring in the ternary alloy, although the local environment of each component, as selected by scanning the photon energy across threshold, is affected by alloying. It occurs a higher delocalisation of the two holes in the valence band than that of the pure components of the alloy, and the coupling between filled and empty states at resonance is consequently modified. According to our data, the need of a high partial density of 3*d* states above the Fermi level is not at all stringent to obtain an intense resonant emission, but rather, the presence of localised quasistationary intermediate states is essential. In fact, the number of empty 3*d*-states in the local DOS of Cr is much higher than Ni and the resonance at the Ni site is more intense than that at Cr site.

5 Summary and conclusions

Our study represents the first application of resonant photoemission to $Fe_{62}Ni_{20}Cr_{18}$ ternary alloy. The results show that atomic-like effects are modified at the Cr, Ni and Fe sites with respect to the pure metals.

The valence band spectra of $Fe_{62}Ni_{20}Cr_{18}$ show a resonant enhancement of the Cr, Fe, Ni satellites at the edges of Cr, Fe and Ni, respectively. For each component, the energy degeneracy of the valence band photoemission satellite and the RR de-excitation channel opening at the $2p_{3/2}$ core level threshold, allows us to locate the

satellite by the resonant enhancements observed at these edges. These satellites turn into Auger structures as soon as the photon energy is scanned across the $2p_{3/2}$ core level thresholds in $Fe_{62}Ni_{20}Cr_{18}$, similar to the pure elements.

The satellite binding energy positions in the alloy change with respect to pure metals. Notably, changes are also observed by looking at the photon energy of the crossover between the Radiationless Raman regime and the Auger emission. Cr and Fe show the crossover below the absorption maximum as seen in pure metals, instead Ni has the crossover at the absorption maximum in pure Ni and below it in the alloy. This difference suggests several effects: the presence of more than one hole in Ni, a partial charge transfer towards the other metals, changes of the hole correlation energies as well as of the electronic structure built by the hetero-nuclear bond formation.

The alloy formation also modifies the intensity of the resonant emission at the Ni, Fe and Cr $2p_{3/2}$ core level thresholds. In particular, Ni $2p_{3/2}$ satellite intensity is reduced, while the Fe intensity is enhanced if compared to pure elements, showing that the behaviour of the resonance at Ni and Fe $2p_{3/2}$-edges in the alloy is considerably different from pure metals.

All species are affected by alloying through a local DOS redistribution, but a charge transfer is likely to occur mainly from Ni to Fe. Charge transfer occurring upon alloying modifies the dynamical properties of the system influencing the satellite binding energies and intensities. In conclusion the differences found in the VB resonant behaviour of $Fe_{62}Ni_{20}Cr_{18}$ at the Fe, Cr, Ni $2p$ absorption edges with respect to each other and to the pure metals, might be due to a combination of charge transfer and multi electron processes.

We thank INFM for economic support during the stage at Elettra.

References

1. F. Besenbacher, I. Chorkendorff, B.S. Clausen, B. Hammer, A.M. Molenbroeck, J.K. Nørskov, I. Stensgaard, Science **279**, 1913 (1998)
2. J.A. Rodriguez, D.W. Goodman, Science **257**, 897 (1992)
3. Y. Gauthier, M. Schmid, S. Padovani, E. Lundgren, V. Buš, G. Kresse, J. Redinger, P. Varga, Phys. Rev. Lett. **87**, 036103 (2001)
4. M. Weinert, R.E. Watson, Phys. Rev. B **51**, 17168 (1995)
5. R. Wu, A.J. Freeman, Phys. Rev. B **52**, 12419 (1995)
6. I.A. Abrikosov, W. Olovsson, B. Johansson, Phys. Rev. Lett. **87**, 176403 (2001)
7. M.V. Ganduglia-Pirovano, J. Kudrnovsky, M. Scheffler, Phys. Rev. Lett. **78**, 1807 (1997)
8. W. Drube, R. Treusch, G. Materlik, Phys. Rev. Lett. **74**, 42 (1995)
9. C. Guillot, Y. Ballu, J. Paigné, J. Lecante, K.P. Jain, P. Thiry, R. Pinchaux, Y. Petroff, L.M. Falicov, Phys. Rev. Lett. **39**, 1632 (1977)
10. O. Tjernberg, S. Söderholm, U.O. Karlsson, G. Chiaia, M. Qvarford, H. Nylen, F. Lindau, Phys. Rev. B **53**, 10372 (1996)
11. L.H. Tjeng, C.H. Chen, J. Ghijsen, P. Rudolf, F. Sette, Phys. Rev. Lett. **67**, 501 (1991)
12. T. Åberg, Phys. Scr. T **41**, 71 (1992)
13. O. Karis, A. Nilsson, M. Weinelt, T. Wiell, C. Puglia, N. Wassdahl, N. Mårtensson, M. Samant, J. Stöhr, Phys. Rev. Lett. **76**, 1380 (1996)
14. U. Fano, Phys. Rev. **124**, 1866 (61)
15. G.B. Armen, H. Wang, Phys. Rev. A **51**, 1241 (1995)
16. M. Weinelt, A. Nilsson, M. Magnuson, T. Wiell, N. Wassdahl, O. Karis, A. Föhlisch, N. Mårtensson, J. Stöhr, M. Samant, Phys. Rev. Lett. **78**, 967 (1997)
17. S. Hüfner, S.H. Yang, B.S. Mun, C.S. Fadley, J. Schäfer, E. Rotenberg, D.D. Kevan, Phys. Rev. B **61**, 12582 (2000)
18. M. Finazzi, N.B. Brookes, F.M.F. de Groot, Phys. Rev. B **59**, 9933 (1999)
19. A. Föhlisch, O. Karis, M. Weinelt, J. Hasselström, A. Nilsson, N. Mårtensson, Phys. Rev. Lett. **88**, 027601 (2002)
20. L. Floreano, G. Naletto, D. Cvetko, R. Gotter, M. Malvezzi, L. Marassi, A. Morgante, A. Santaniello, A. Verdini, F. Tommasini, G. Tondello, Rev. Sci. Instrum. **70**, 3855 (1999)
21. R. Gotter, A. Ruocco, A. Morgante, D. Cvetko, L. Floreano, F. Tommasini, G. Stefani, Nucl. Instrum. Methods A **467-468**, 1468 (2001)
22. J.J. Yeh, I. Lindau, Atomic Data and Nuclear Data Tables **32**, 1 (1985)